

Numerical Investigation of the Flexure Behavior of Reinforced Concrete Spandrel Beams with Distributed Tension Reinforcement

Rafaa M. Abbas*

Assistant Professor

College of Engineering-University of Baghdad
Iraq, Baghdad

Email: dr.rafaa@coeng.uobaghdad.edu.iq

Wesal A. Fadala

M.Sc. student

College of Engineering-University of Baghdad
Iraq, Baghdad

Email: w.ameen1101@coeng.uobaghdad.edu.iq

ABSTRACT

When the flange of a reinforced concrete spandrel beam is in tension, current design codes and specifications enable a portion of the bonded flexure tension reinforcement to be distributed over an effective flange width. The flexural behavior of the RC L-shaped spandrel beam when reinforcement is laterally displaced in the tension flange is investigated experimentally and numerically in this work. Numerical analysis utilizing the finite element method is performed on discretized flanged beam models validated using experimentally verified L-shaped beam specimens to achieve study objectives. A parametric study was carried out to evaluate the influence of various factors on the beam's flexure behavior. Results showed that as the percentage of the reinforcement distributed has increased over a greater width of the flange, a considerable drop in beam flexure strength was observed with excessive deflection. According to the study, not more than 33% of the web tension reinforcement might be distributed over an effective flange width less than $l_n/10$, including the web region, as recommended by the ACI318-14.

Keywords: Reinforced concrete, spandrel beam, flexure strength, finite element, deflection

التحقق العددي لسلوك الانثناء للاعتاب الخرسانية المسلحة الطرفية مع توزيع حديد الشد

وصال أمين فضالة
طالبة ماجستير
كلية الهندسة – جامعة بغداد

*رافع محمود عباس
استاذ مساعد
كلية الهندسة – جامعة بغداد

الخلاصة

عندما تكون شفة الاعتاب الخرسانية المسلحة الطرفية في حالة شد، فإن مدونات التصميم والمواصفات الحالية تتيح توزيع جزء من حديد الشد للانثناء على عرض شفة فعال. تم دراسة سلوك الانثناء للاعتاب الخرسانية المسلحة ذات الشكل L عند انتشار قضبان حديد التسليح بشكل جانبي في شفة الشد تجريبياً وعددياً في هذا العمل. تم إجراء التحليل العددي باستخدام طريقة العناصر

*Corresponding author

Peer review under the responsibility of University of Baghdad.

<https://doi.org/10.31026/j.eng.2022.03.02>

2520-3339 © 2022 University of Baghdad. Production and hosting by Journal of Engineering.

This is an open access article under the CC BY4 license <http://creativecommons.org/licenses/by/4.0/>.

Article received: 17/8/2021

Article accepted: 3/10/2021

Article published: 1/3/2022



المحددة على نماذج الاعتاب ذات الشفة التي تم التحقق من صحتها باستخدام نماذج اعتاب تم التحقق منها تجريبياً لتحقيق الهدف. تم إجراء دراسة مقارنة لتقييم تأثير العوامل المختلفة على سلوك الانحناء للاعتاب. بينت النتائج انه بزيادة كمية توزيع حديد التسليح على عرض واسع من الشفة، لوحظ انخفاض كبير في قوة انثناء العارضة مع زيادة مهمة في الهطول. وفقاً للدراسة، يجب توزيع ما لا يزيد عن 33% من حديد الشد على عرض شفة فعال أقل من $\ln/10$, وكما توصي المدونة الامريكية ACI318. **الكلمات الرئيسية:** الخرسانة المسلحة، الاعتاب الطرفية، قوة الانثناء، عناصر محدودة، الهطول

1. INTRODUCTION

T and L-Shaped flanged beams are commonly encountered in usual construction. They are mostly seen in framed structures and are often used as part of the moment-resisting frames. Because slabs are cast monolithically with the web of the beam, the rectangular beam section gains additional stiffness or strength as a result of the slab's participation (**Darwin et al., 2015**). Intermediate beams, which have slabs on both sides, commonly act as T-beams. The edge beams and the beams around staircase or lift openings, which have slabs only on one side, act as L-beams. A portion of the slab works integrally with the beam in both T-beams and L-beams. As a result, this slab section bends in the same direction as the beam bends. Hence, one can define the effective flange as the part of the slab above the beam's web.

Most recently, the flexure behavior of flanged RC beams has been the subject of many research efforts (**Cladera, et al., 2015, González and Ruiz, 2017, Shaaban, et al., 2017**). **Bousalem, et al., 2017** investigated the flexural behavior of RC rectangular and T-beams strengthened with CFRP laminates using NSM technique and to provide direct analysis method for the evaluation of the flexural strength of FRP reinforced concrete beams. The analysis is based on common principles of equilibrium equation and compatibility of strains. The developed equations were compared with experimental results available in the literature and proven the effectiveness of the presented design equations for estimating the flexural capacity of the investigated sections strengthened with CFRP laminates strips. **Pohoryles, et al., 2021** investigated the combined shear and flexural strengthening of RC T-beams using fibre-reinforced polymer sheets and textile reinforced mortars. Twelve retrofitted reinforced concrete beams were tested to study the retrofit effectiveness and the difference in efficiency of the two strengthening techniques considering the effect of the reinforcement ratio, the amount of composite material used and the effect of the shear span. The results of the FE model were used to perform parametric study to further study the effect of the investigated parameters on the retrofit effectiveness.

Because the slab and the beams are, generally, monolithically cast, the slab's contribution to the beam's strength may be considered. The effective flange is part of the slab that adds to beam strength (**McCormac and Brown, 2015**). Shearing deformation of the flange relieves some compressive stress on the more remote parts, i.e., the shear-lag phenomenon. Variable compressive stresses acting on the overall width can be replaced by a uniformly distributed compressive force acting on the effective width, as determined by design procedures (**Abbas and Shaker, 2015, Qin, et al., 2014**). Hence, the effective width of the flange is the width of a hypothetical flange that compresses uniformly across its width by the same amount as the loaded edge of the real flange under the same edge shear forces.

Although many studies on reinforced concrete T-beams have been conducted in past decades, studies on the negative moment regions of continuous T beams and L-beams are uncommon. In terms of the influence of the lateral distribution of the flexure rebars in the tension flange, no research has been conducted so far. Therefore, this study aims to address a practical issue that



arises in usual practice when bonded tension reinforcement is distributed in the tension flanges of L-shaped beams as allowed by the (ACI 318M-19) design code to protect the flange's outer parts from excessive flexure cracks. The influence of tension reinforcement distribution will be discussed and highlighted when the flexural behavior of such beams is investigated.

2. RESEARCH METHODOLOGY

To accomplish the study objectives, full-scale reinforced concrete L-beam models representative of the slab-beam system in common structures were examined. Using Abaqus CAE software, a 3-D finite element model has been used to depict and discretize the idealized L-beams with effective flanges. To that purpose, the created finite element models were tentatively verified by comparing them to the experimental results obtained in this study on a scaled-down L-beam model. The results of the intensive numerical research were then presented to evaluate the effect of the distributed steel rebar locations, percentages, and different parameters on the flexural behavior of the L-beam models under consideration.

3. BEAM MODEL

The current study adopted a typical exterior reinforced concrete L-beam representative of a full-scale reinforced concrete slab-edge beam system to investigate the problem under consideration, as shown in **Fig. 1**. The adopted L-beam model with a clear span of $L_n=5$ m, effective flange width $b_f=0.7$ m, and slab thickness $h_f=0.150$ m was reinforced with 6#20 steel rebars in the tension flange section. The shear reinforcement consisted of #12 stirrups spaced at a distance of 150 mm. The total depth of the beam $h=0.50$ m.

The suggested tension reinforcement is located in the beam flange to simulate tension in the flange in the case of the section subjected to the negative moment at the support regions in continuous beams or mid-span reinforcement for inverted beams with the flange beneath the beam stem. The selected effective flange width of 0.7m was calculated in accordance with the limitation stipulated in **Table 6.3.2.1** of the **ACI318M-2019** for the indicated slab dimensions.

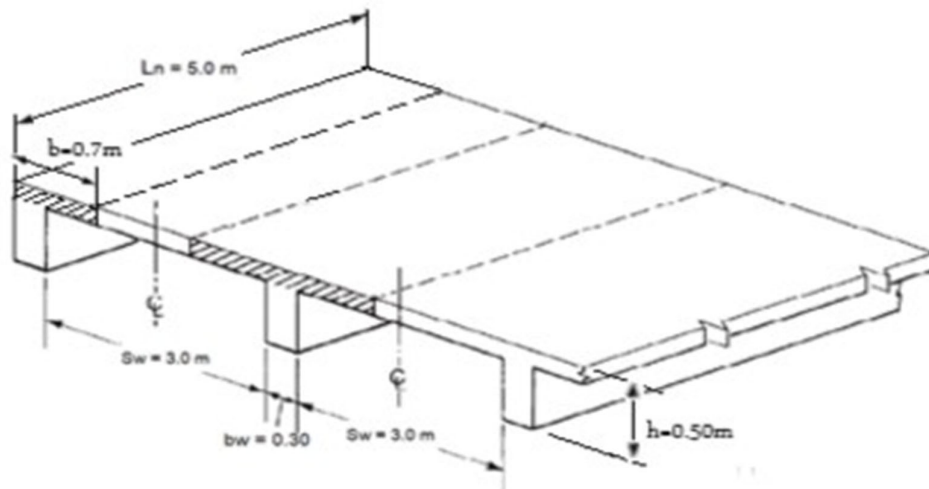


Figure 1. (A) Slab-Beam model.

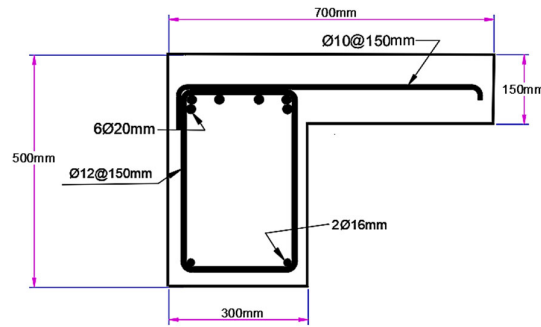


Figure 1. (B) L-Beam model section details.

To achieve the study's goals, the modeled beam was numerically simulated as a simply supported beam with the flange situated under the beam web. The beam idealization shown in **Fig.2** helps to mimic the case of tension in the flange as used in the experimental testing program that was used to validate the finite element model results. Beam reinforcement of 6#20 bars and stirrups were selected to ensure flexure failure due to concentrated mid-span load.

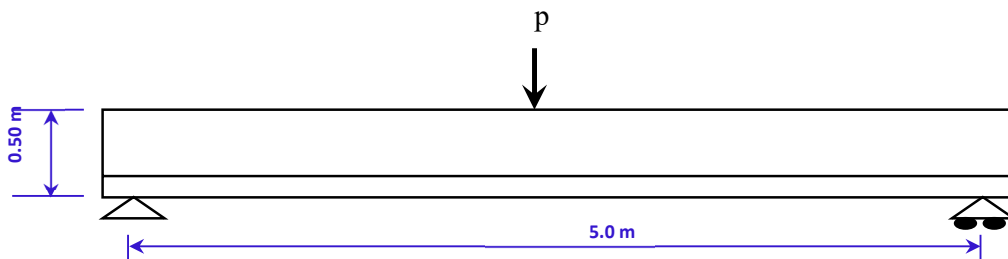


Figure 2. L-beam schematic representation.

4. FINITE ELEMENT MODEL

The numerical finite element model used in this investigation is presented in this section. Any structural analysis requiring FE modeling must include all structural aspects necessary for determining the load-deflection characteristics, which provides crucial information about the structure's stiffness and strength. These include; the geometry of the problem, including span, member cross-sections, boundary conditions, as well as material mechanical properties and active loads.

Three-dimensional finite element models have been prepared and calibrated using the results of the experimental work. Abaqus CAE 6.19 software has been used in the modeling process (Simulia, 2013). **Fig. 3** shows the FE model of the L-beam model adopted in the numerical analysis. In the part module, Abaqus features can be used to simulate different structural geometry. To represent the concrete section, a solid 8-node brick element (C3D8R) is used to simulate the concrete section in the beam web and flange. On the other hand, a three-dimensional wire truss element is used to simulate the longitudinal and stirrup reinforcements.

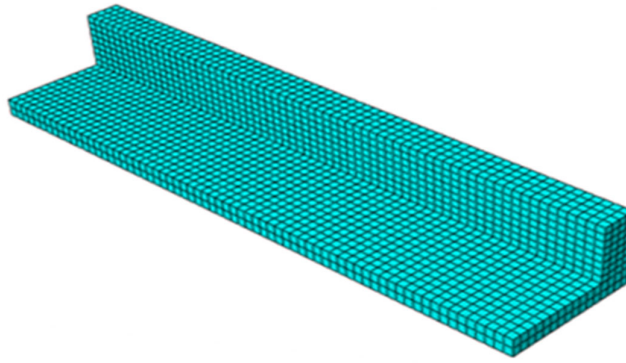


Figure 3. Discretized L-beam finite element model.

Nonlinear finite element analysis was performed to simulate the actual nonlinear behavior of the concrete structures. Concrete Damaged Plasticity, or CDP, was used to account for the plasticity features of the concrete material. Using the interaction module, part modules must be connected to facilitate the successful assembly of the various components. To ensure a perfect connection with the surrounding concrete, embedded restrictions were used for the reinforcing rebars. To work in a linked form, part instances must be joined together.

4.1 Plasticity Parameters

Material modeling of the concrete passes through two steps. The first one is the elastic model in which the modulus of elasticity and Poisson's ratio were defined. The second one is the damage plasticity model used to describe the nonlinear portion of the stress-strain curve of the concrete. Plasticity has five parameters that must be defined to solve the plastic flow and yield function (Table 1).

Table 1. Concrete Damaged Plasticity model parameters.

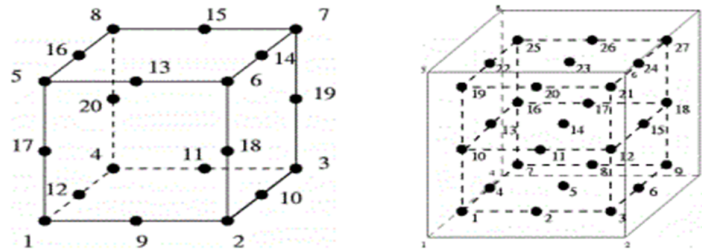
Plasticity parameters	
Dilation angle	30
Eccentricity	0.1
f_{b0}/f_{c0}	1.16
Viscosity parameter	0.667
kc parameter	0.0001

4.2 Modeling of the beam elements

In ABAQUS, there are two integration rules: the reduced Gauss-quadrature integration (2x2x2) and the complete Gauss-quadrature integration (3x3x3). The three-dimensional twenty-node linear brick element with decreased integration and hourglass control (C3D20R) was used for the concrete (Ahmed, 2014). The (C3D20) elements are quadratic brick elements that may be used in any situation (with 3x3x3 integration points). However, there are different varieties of three-dimensional elements. The nodes' numbering follows a standard pattern as shown in Fig. 4a and the integration scheme as given in Fig. 4b. Also, in this work, beam reinforcement was modeled as axial members (A 2-node linear 3D truss element) inserted within the concrete element,



resulting in a perfect connection between the steel bars and the concrete, as shown in Fig. 5 . Quadratic elements were used to simulate the bearing plates at the bottom of the model and under the applied load (full touch element with the complete connection between the bearing plates and the specimen).



(a). 20-node brick element (b). 3x3x3 integration point scheme in hexahedral elements

Figure 4. The C3D20 element (Simulia, 2014).

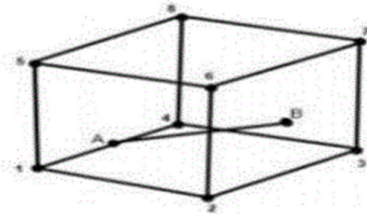


Figure 5. Truss element (AB) embedded in 3D continuum element (Simulia, 2014).

5. VALIDATION OF THE FE MODEL

Because experimental testing is time-consuming and costly, whereas finite element analysis is quicker and less expensive, a finite element model was created to analyze the flexural behavior of the reinforced concrete L-beams in this work. To verify and check the accuracy of the proposed FE model, comparison with experimental specimen results was checked and validated. One simply supported RC L-beam specimen was cast and tested as part of this study and was used to approve the numerical model adequacy. The details of the examined beam models are shown in Fig. 6.

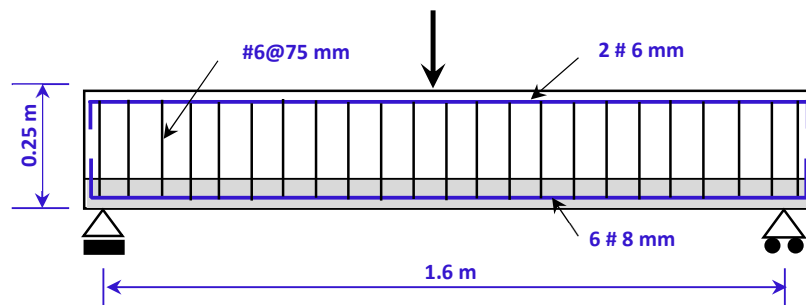


Figure 6. Tested L-beam (LB400) specimen details.

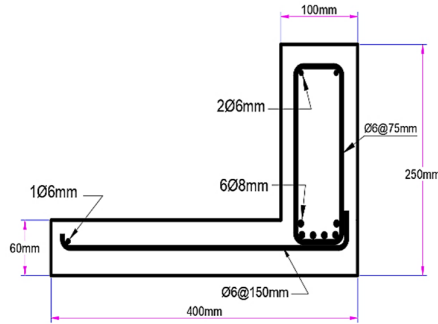


Figure 6. Continued.

The tested beam spanned 1700 mm and was made from concrete with a compressive strength of 25 MPa. The beam was reinforced with 6 Φ 8mm bars as the main reinforcement, 2 Φ 6mm as nominal rebars in the compression side, whereas Φ 6mm@75 mm centers as stirrups for shear reinforcement. The selected reinforcement and beam features were to ensure tension control failure. The tested beam is a scaled-down RC beam specimen with an $a/d = 3.5$ shear span-to-depth ratio. Finally, the tested beam specimen and setup shown in **Fig. 7** was designed to model the problem of flexure tension in the flange of L-beam investigated in this work. Also, **Fig. 7** shows the crack pattern and deformation of the L-beam specimen at failure.

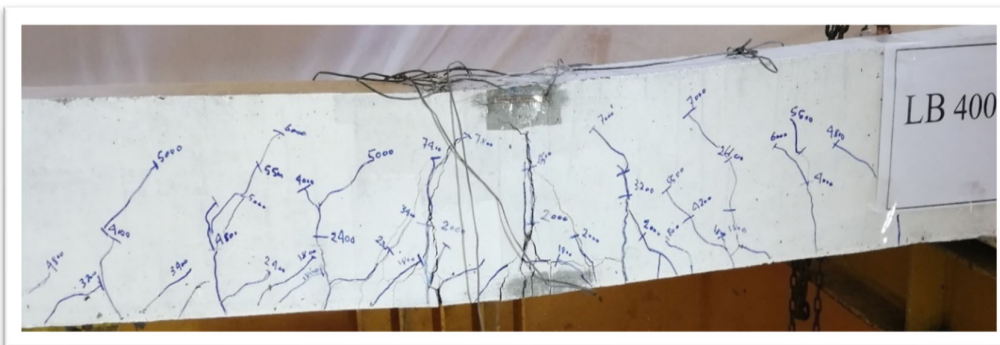


Figure 7. Testing setup and cracking for L-beam (LB400) specimen.



Comparison for the load-deflection results of the tested beam specimen and the finite element model for the tested beam is presented in Fig. 8. The results revealed that the deflection and ultimate load calculated using the finite element approach matched closely those obtained experimentally. Validation ratios for the ultimate load capacity and deflection for the FE model and experimental results are compiled in Table 2. Results showed that the finite element approach could produce accurate analytical results equivalent to those obtained experimentally.

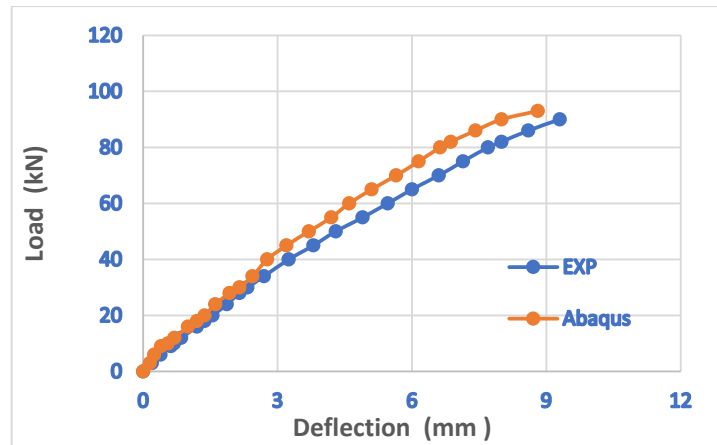


Figure 8. Experimental and finite element load-deflection curves for LB400 specimen.

Table 2 Comparison of the experimental and FE results.

Beam designation	Finite Element results		Experimental results		Validation ratio %	
	$P_{u, FE}$ (kN)	Δ_{FE} (mm)	$P_{u, EXP}$ (kN)	Δ_{EXP} (mm)	Strength	Deflection
LB400	93	8.81	90	9.3	3.4%	5.2%

The results indicated that the experimental deflection values were greater than those obtained using the finite element model. The experimental specimen exhibited more ductile behavior at failure than the FE model of the identical L-beam. These percentages show that the finite element nonlinear analysis results are similar to those found experimentally.

6. PARAMETRIC STUDY

The validated finite element simulation was utilized in this section to carry out a comprehensive numerical analysis to evaluate the structural behavior of the reinforced concrete spandrel beams when part of the flexure reinforcement is distributed in the tension flange. Moreover, the impact of three factors, namely effective flange thickness, concrete compressive strength, and total beam depth, have been incorporated in the numerical model to address all the factors that might influence the flexural behavior of these beams.

Three different values of the effective flange thickness (100, 150, 200 mm), three different values of the concrete compressive strength (20, 30, 40 MPa), and three different values of the beam depth (400, 500, 600 mm) have been considered. All other mechanical properties of the model



were kept at their average values for each parameter when one parameter was evaluated. Two additional features must be justified to comply with the ACI 318 code recommendation: the portion or percentage of web reinforcement to be spread in the flange and the width of the effective flange, which is required to accommodate the distributed rebars.

Finally, **LB-xx (x)** represents the designation adopted for the numerical beam models. Hence, **LB** holds for the spandrel beam, **(xx)** for the percentage of the distributed rebars, and **(x)** stands for the width of the effective flange over which reinforcement to be distributed as part of the beam span.

Table 3 shows beam model properties investigated numerically in this study by using the adopted finite element analysis.

Table 3. Beam model properties used for the parametric study.

Parameter considered	Beam Properties					
	Beam designation	Length (mm)	Flange width (mm)	Beam depth (h) mm	Compressive Strength f_c' (MPa)	h_f (mm)
<i>Flange thickness (h_f)</i>	LB-0	5000	700	500	30	(100, 150, 200)
	LB-33(1)	5000	700	500	30	
	LB-33(2)	5000	700	500	30	
	LB-50 (1)	5000	700	500	30	
	LB-50(2)	5000	700	500	30	
<i>Compressive Strength f_c'</i>	LB-0	5000	700	500	(20, 30, 40)	150
	LB-33(1)	5000	700	500		150
	LB-33(2)	5000	700	500		150
	LB-50(1)	5000	700	500		150
	LB-50(2)	5000	700	500		150
<i>Beam depth (h)</i>	LB-0	5000	700	(400, 500, 600)	30	150
	LB-33(1)	5000	700		30	150
	LB-33(2)	5000	700		30	150
	LB-50(1)	5000	700		30	150
	LB-50(2)	5000	700		30	150

In the beam designation adopted, **(xx)** for the part or percentage of the flexure rebars distributed was taken **0%, 33%, and 50%** of the overall web reinforcement, whereas the **(x)** designation for the width of the effective flange used to distribute tension rebars was taken; **(1)** for reinforcement distributed over width not wider than $l_n/10$, and **(2)** reinforcement distributed over width wider than $l_n/10$. The ACI 318 recommended flange width limitation for reinforcing distribution was used. **Fig. 9** depicts the cross-section of the L-shaped spandrel beam with the reinforcement distribution scheme compiled in **Table 3**. It's worth noting that the beam models were tested as a



simply supported beam with the flange under the beam web, i.e., the tension in the flange, to simulate the case of tension in the flange, as shown in Fig. 2.

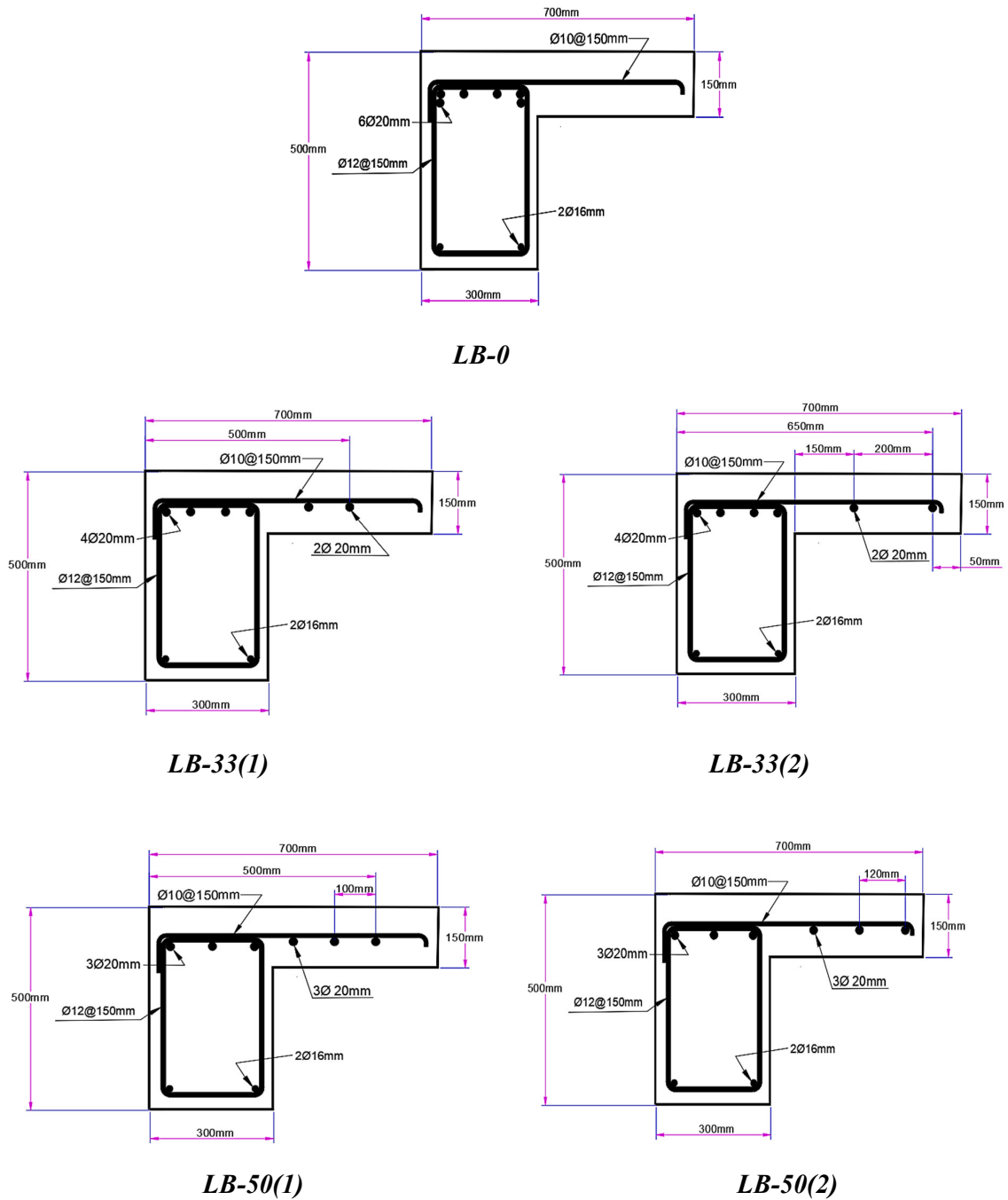


Figure 9. Spandrel beam cross-section and reinforcement distribution details.



Figs. 10, 11, and 12 show the load-deflection curves for the investigated beams with the different parameters listed in Table 3. On the other hand, Tables 4, 5, and 6 show the variation percentages in the spandrel beam behavior for the ultimate load and deflections values related to the influence of the parameters inspected and the part of the flexure reinforcement distributed in the specified effective flange width. Finally, it is noted that beam model "LB-0" was used as the reference beam in this investigation.

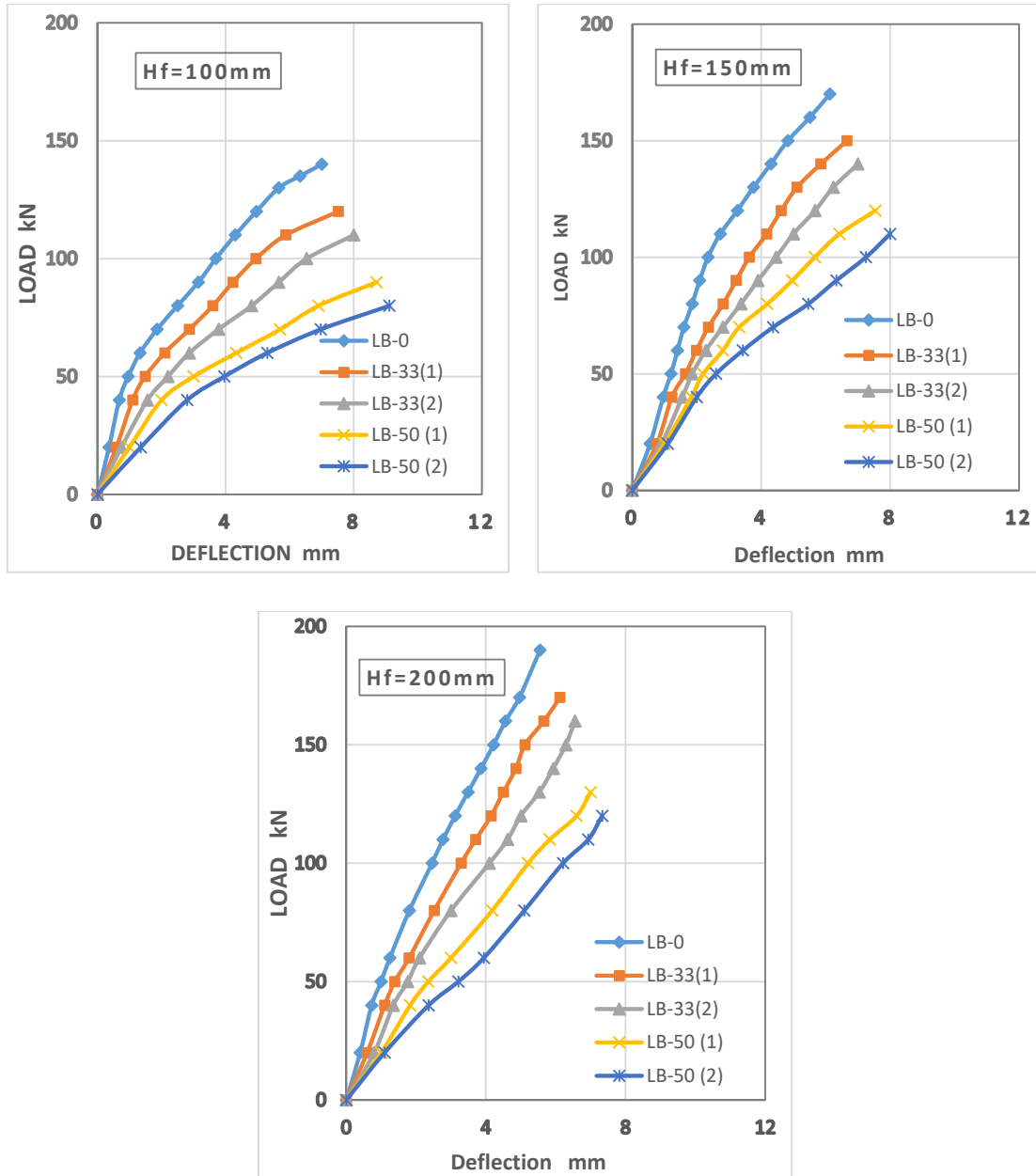


Figure 10. Load-deflection curves for the spandrel beams for different flange thickness.

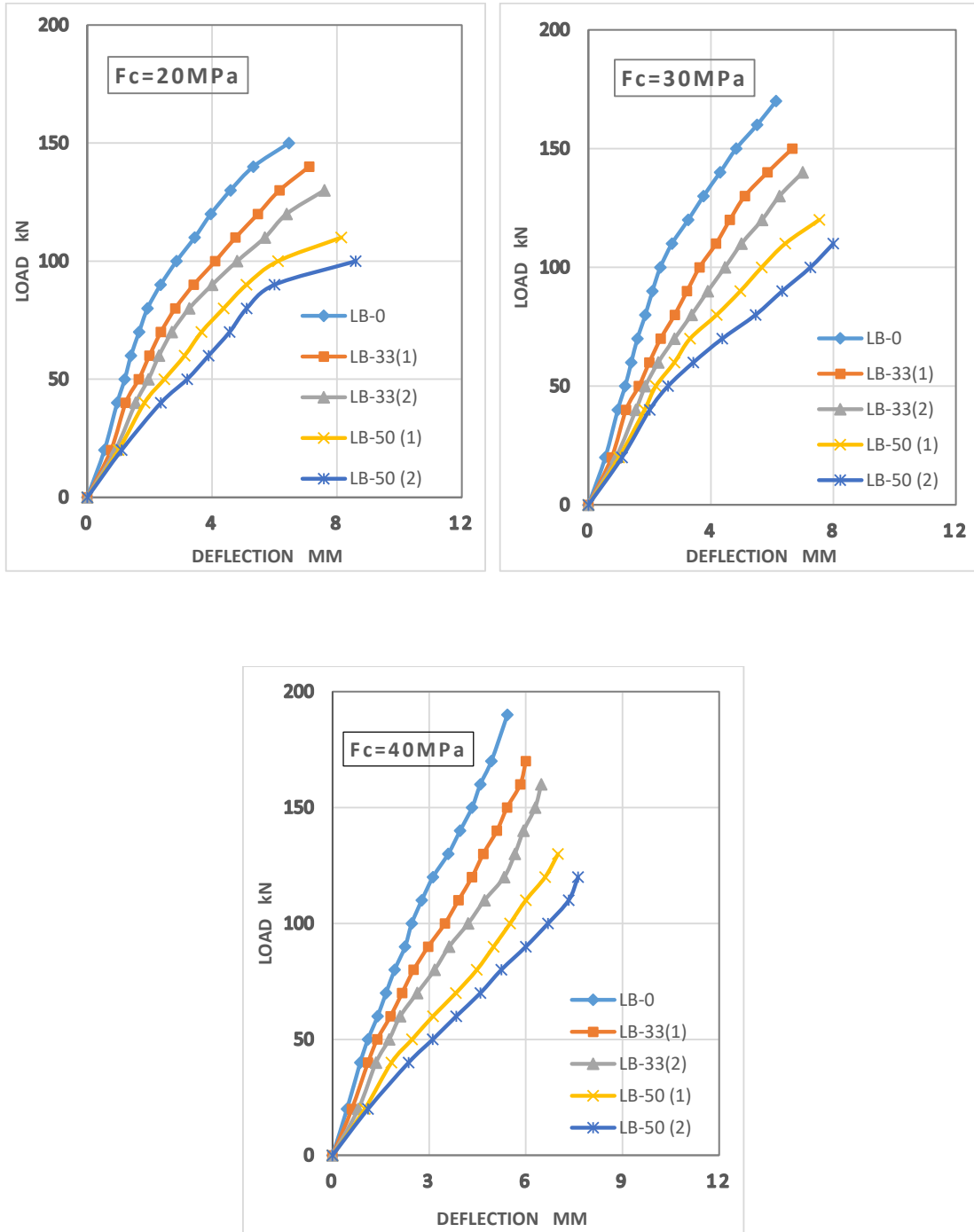


Figure 11. Load-deflection curves for the spandrel beams for different concrete compressive strengths.

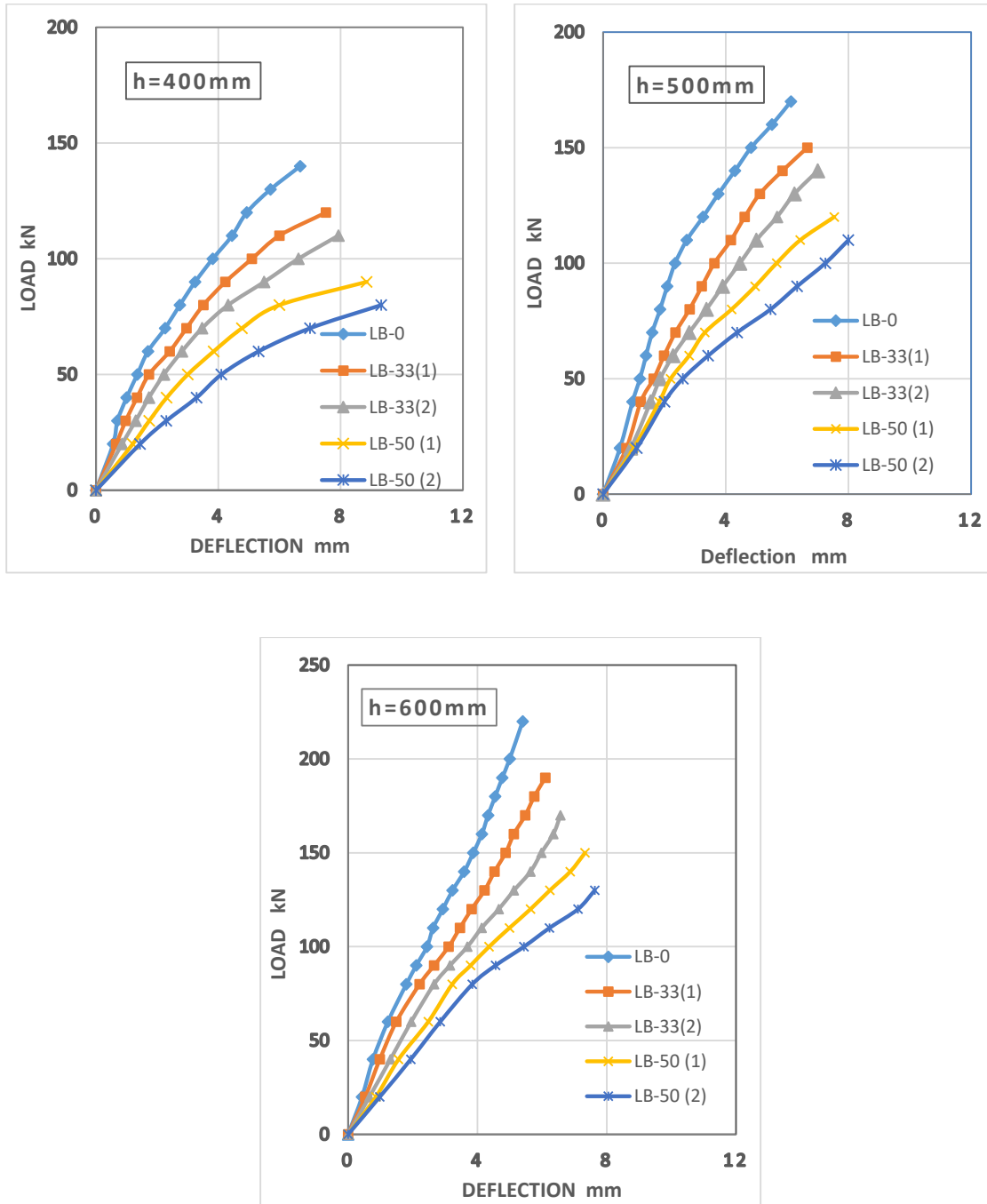


Figure 12. Load-deflection curves for the spandrel beams for different beam depth.

**Table 4.** Variation percentages in the spandrel beam behavior for different flange thickness.

Beam designation	FE Analysis Results		Variation ratio (%)	
	Maximum Load P_u (kN)	Max. deflection Δ (mm)	Strength	Deflection
Flange thickness = 100mm				
LB-0	138	7	----	----
LB-33(1)	120	7.52	-13.0	7.4
LB-33(2)	110	8	-20.3	14.3
LB-50(1)	88	8.71	-36.2	24.4
LB-50(2)	80	9.11	-42.0	30.1
Flange thickness = 150mm				
LB-0	170	6.13	----	----
LB-33(1)	148	6.66	-12.9	8.6
LB-33(2)	140	7	-17.6	14.2
LB-50(1)	119	7.54	-30	23.0
LB-50(2)	112	8	-34.0	30.5
Flange thickness = 200mm				
LB-0	190	5.55	----	----
LB-33(1)	173	6.12	-8.9	10.3
LB-33(2)	156	6.55	-17.9	18.0
LB-50(1)	130	7	-31.6	26.1
LB-50(2)	120	7.33	-36.8	32.1

Table 5. Variation percentages in the spandrel beam behavior for different concrete compressive strength.

Beam designation	FE Analysis Results		Variation ratio (%)	
	Maximum Load P_u (kN)	Max. deflection Δ (mm)	Strength	Deflection
Concrete compressive strength = 20 MPa				
LB-0	152	6.64	----	----
LB-33(1)	143	7.11	-5.9	7.1
LB-33(2)	130	7.6	-14.5	14.4
LB-50(1)	118	8.14	-22.3	22.6
LB-50(2)	102	8.6	-32.9	29.5
Concrete compressive strength = 30 MPa				
LB-0	170	6.13	----	----
LB-33(1)	167	6.66	-12.9	8.6
LB-33(2)	140	7	-17.6	14.2



LB-50(1)	119	7.54	-30	23.0
LB-50(2)	112	8	-34.0	30.5
Concrete compressive strength = 40 MPa				
LB-0	190	5.43	----	----
LB-33(1)	172	6	-9.5	10.5
LB-33(2)	160	6.48	-15.8	19.3
LB-50(1)	128	7	-32.6	28.9
LB-50(2)	120	7.62	-36.8	40.3

Table 6. Variation percentages in the spandrel beam behavior for different beam depth values.

Beam designation	FE Analysis Results		Variation ratio (%)	
	Maximum Load P_u , (kN)	Max. deflection Δ (mm)	Strength	Deflection
Beam depth = 400 mm				
LB-0	140	6.68	----	----
LB-33(1)	121	7.52	-13.6	12.5
LB-33(2)	110	7.93	-21.4	18.7
LB-50(1)	95	8.85	-32.1	32.5
LB-50(2)	80	9.33	-42.8	39.7
Beam depth = 500 mm				
LB-0	170	6.13	----	----
LB-33(1)	148	6.66	-12.9	8.6
LB-33(2)	140	7	-17.6	14.2
LB-50(1)	119	7.54	-30.0	23.0
LB-50(2)	112	8	-34.0	30.5
Beam depth = 600 mm				
LB-0	223	5.4	----	----
LB-33(1)	191	6.1	-14.3	12.9
LB-33(2)	174	6.57	-21.9	21.7
LB-50(1)	155	7.33	-30.5	35.7
LB-50(2)	130	7.63	-41.7	41.3

To evaluate the results presented in the aforementioned tables, a summary of the outcomes from the analyses results was compiled in **Tables 7 and 8**. **Table 7** presents a summary for the ranges of the minimum and maximum variation percentages in the ultimate load and the maximum deflection values resulting from the effect of reinforcement distribution and for the different parameters considered. In this table, the minimum range presented is for the L-beam model “**LB-33(1)**”, minimum distributed percentage over width $\leq \ell n/10$, while the maximum range presented is for the L-beam model “**LB-50(2)**”, maximum distributed percentage over width $> \ell n/10$. Results presented in **Table 7** revealed that a maximum reduction in the ultimate load capacity of about 9%



and a maximum increase in the maximum deflection of about 11% had been observed due to the effect of the flange thickness, concrete compressive strength, or beam depth. Generally, the impact of the three parameters considered was less than 5% for the most case study presented in **Tables 4, 5, and 6**, indicating a minimal effect for the parameters considered on the flexure behavior of the spandrel beams with distributed rebars.

Table 7. Ranges for the variation percentages in the L-beam flexure behavior.

Parameters considered	% Reduction in the ultimate load		% Increase in the max. deflection	
	Min. range	Max. range	Min. range	Max. range
Flange thickness (100, 150, 200) mm	8.9 – 13.0	34.0 – 42.0	7.4 – 10.3	30.1 – 32.1
Concrete Strength (20, 30, 40) MPa	5.9 – 12.9	32.9 – 36.8	7.1 – 10.5	29.5 – 40.3
Beam depth (400, 500, 600) mm	12.9 – 14.3	34.0 – 42.8	8.6 – 12.9	30.5 – 41.3

The average percentages for the decrease or increase in the ultimate load capacity and maximum deflection are due to the combined impact of the percentage of the distributed reinforcement, the width of the effective flange over which rebars distributed, and the three parameters considered were summarized in **Table 8**. Results presented in this table revealed that the percentage of reinforcement and the width over which rebars to be distributed were the most effective factors influencing the flexure behavior of L-beams with distributed reinforcement. A minimum variation percentage of about 10% was noticed when 33% of tension rebars distributed over flange width $\leq \ell n/10$, whereas this percentage increased up to about 37% when 50% of tension rebars were distributed over flange wider flange width.

Table 8. Summary of the average variation percentages in the spandrel beam flexure behavior.

Parameters considered	% Reduction in the ultimate beam load	% Increase in the beam max. deflection
Reinforcement distributed, 33% Effective width, $\leq \ell n/10$	10.1	10.0
Reinforcement distributed, 33% Effective width, $> \ell n/10$	18.0	17.9
Reinforcement distributed, 50% Effective width, $\leq \ell n/10$	31.2	29.1
Reinforcement distributed, 50% Effective width, $> \ell n/10$	37.8	35.5



7. CONCLUSIONS

From the results presented in this study, the following conclusions can be drawn:

- The study revealed that the nonlinear finite element approach could produce accurate numerical results comparable to those obtained experimentally.
- The finite element results showed that the experimental beam model exhibited more ductile behavior at failure than the FE model of the identical spandrel beam.
- The study indicated that when part of the tension reinforcement was distributed in the spandrel beam flange, the ultimate load decreased and the maximum deflection at failure increased and that the variation in the results increased as more rebars were displaced in a wider flange section.
- Results showed that the three parameters considered in this study, i.e., flange thickness, concrete compressive strength, and beam depth, have minimal effect on the flexure behavior of the spandrel beams when part of the flexure rebars is distributed in the beam flange.
- The part or percentage of the distributed reinforcement and the width of the effective flange used to distribute rebars was found to be the most effective factors affecting the flexure behavior of spandrel beams with distributed rebars.
- A minimum variation percentage of about 10% in the beam's flexural behavior was noticed when 33% of the tension rebars distributed over a flange width less than $\ell_n/10$. In contrast, this percentage increased up to about 37% when 50% of the tension rebars distributed over flange width wider than $\ell_n/10$.
- To limit the decrease in beam flexure strength, the study recommended that not more than 33% of the tension reinforcement might be distributed across an effective flange width not wider than $\ell_n/10$.

Acknowledgment

The authors gratefully acknowledge the Department of Civil Engineering at the University of Baghdad for their valuable help in completing this work. The authors would like to thank the support received from the head and the staff of the Department.

REFERENCES

- Darwin, D., Dolan, C., and Nilson, A., 2015. Design of Concrete Structures. 15th Edition, McGraw Hill.
- Cladera, A., Marí, A., Ribas, C., Bairán, J., and Oller, E., 2015. Predicting the shear-flexural strength of slender reinforced concrete T and I shaped beams. Eng. Struct. 101, 386-396, <http://dx.doi.org/10.1016/j.engstruct.2015.07.025>.



- González, C. R., and Ruiz, M. F., 2017. Influence of flanges on the shear-carrying capacity of reinforced concrete beams without web reinforcement, *Int. Federation for Structural Concrete, Str. Con.*, 1-13, [DOI: 10.1002/suco.201600172](https://doi.org/10.1002/suco.201600172).
- Shaaban, I. G., Saidani, M., Nurddin, M. F., Malkawi, A. B., and Mustafa, T. S., 2017. Serviceability behavior of normal and high-strength reinforced concrete T-beams. *Eur. J. Mat. Sci. Eng.* 2, 99-110.
- Bousalem B., Benzaid R., Chikh N., and Mesbah H., 2017. Flexural Analysis of RC Rectangular and T Beams Strengthened with NSM FRP Reinforcement. *I. J. of Civil Eng. and Const. Science*, 4(1): 1-10.
- Pohoryles D.A., Melo J., and Rossetto T., 2021. Combined Flexural and Shear Strengthening of RC T-Beams with FRP and TRM: Experimental Study and Parametric Finite Element Analyses. *Buildings* 11, 520, <https://doi.org/10.3390/buildings11110520>.
- McCormac, J. C., and Brown, R. H., 2015. *Design of Reinforced Concrete*. 10th Edition, John Wiley & Sons.
- Abbas, R. M., and Shaker, H. J., 2015. Finite Element Investigation on Shear Lag in Composite Concrete-Steel Beams with Web Openings. *J. Eng.* 21, 11-33.
- Qin, X. X., Liu, H. B., Wang, S. J. Z., and Yan, h., 2014. Simplistic Analysis of the Shear Lag Phenomenon in a T-Beam. *J. Eng. Mech. (ASCE)* 15, [https://doi.org/10.1061/\(ASCE\)EM.1943-7889.0000882](https://doi.org/10.1061/(ASCE)EM.1943-7889.0000882).
- ACI 318M-19, 2019. *Building Code Requirements for Structural Concrete and Commentary*. an ACI Standard, American Concrete Institution.
- Ahmed, A., 2014. Modeling of a reinforced concrete beam subjected to impact vibration using ABAQUS. Vol. 4, No 3, 0976 – 4399.
- Simulia, 2013. *Abaqus Analysis User's Guide*. Dassault Systèmes Simulia Corp.
- Simulia, 2014. *Getting Started with Abaqus: Interactive Edition*. Dassault Systèmes Simulia Corp.